Atmos. Meas. Tech., 5, 1935–1952, 2012
www.atmos-meas-tech.net/5/1935/2012/
doi:10.5194/amt-5-1935-2012

Atmospheric Measurement Techniques

SCIAMACHY WFM-DOAS XCO_2: comparison with CarbonTracker XCO_2 focusing on aerosols and thin clouds

J. Heymann[1], O. Schneising[1], M. Reuter[1], M. Buchwitz[1], V. V. Rozanov[1], V. A. Velazco[1,*], H. Bovensmann[1], and J. P. Burrows[1]

[1]Institute of Environmental Physics – IUP, University of Bremen FB1, Otto-Hahn-Allee 1, P.O. Box 33 04 40, 28334 Bremen, Germany
[*]now at: School of Chemistry, University of Wollongong, Wollongong, New South Wales, Australia

Correspondence to: J. Heymann (heymann@iup.physik.uni-bremen.de)

Received: 30 March 2012 – Published in Atmos. Meas. Tech. Discuss.: 17 April 2012
Revised: 10 July 2012 – Accepted: 16 July 2012 – Published: 13 August 2012

Abstract. Carbon dioxide (CO_2) is the most important greenhouse gas whose atmospheric loading has been significantly increased by anthropogenic activity leading to global warming. Accurate measurements and models are needed in order to reliably predict our future climate. This, however, has challenging requirements. Errors in measurements and models need to be identified and minimised.

In this context, we present a comparison between satellite-derived column-averaged dry air mole fractions of CO_2, denoted XCO_2, retrieved from SCIAMACHY/ENVISAT using the WFM-DOAS (weighting function modified differential optical absorption spectroscopy) algorithm, and output from NOAA's global CO_2 modelling and assimilation system CarbonTracker. We investigate to what extent differences between these two data sets are influenced by systematic retrieval errors due to aerosols and unaccounted clouds. We analyse seven years of SCIAMACHY WFM-DOAS version 2.1 retrievals (WFMDv2.1) using CarbonTracker version 2010.

We investigate to what extent the difference between SCIAMACHY and CarbonTracker XCO_2 are temporally and spatially correlated with global aerosol and cloud data sets. For this purpose, we use a global aerosol data set generated within the European GEMS project, which is based on assimilated MODIS satellite data. For clouds, we use a data set derived from CALIOP/CALIPSO.

We find significant correlations of the SCIAMACHY minus CarbonTracker XCO_2 difference with thin clouds over the Southern Hemisphere. The maximum temporal correlation we find for Darwin, Australia ($r^2 = 54\,\%$). Large temporal correlations with thin clouds are also observed over other regions of the Southern Hemisphere (e.g. 43 % for South America and 31 % for South Africa). Over the Northern Hemisphere the temporal correlations are typically much lower. An exception is India, where large temporal correlations with clouds and aerosols have also been found. For all other regions the temporal correlations with aerosol are typically low. For the spatial correlations the picture is less clear. They are typically low for both aerosols and clouds, but depending on region and season, they may exceed 30 % (the maximum value of 46 % has been found for Darwin during September to November).

Overall we find that the presence of thin clouds can potentially explain a significant fraction of the difference between SCIAMACHY WFMDv2.1 XCO_2 and CarbonTracker over the Southern Hemisphere. Aerosols appear to be less of a problem. Our study indicates that the quality of the satellite derived XCO_2 will significantly benefit from a reduction of scattering related retrieval errors at least for the Southern Hemisphere.

1 Introduction

Since pre-industrial times, the concentration of the atmospheric greenhouse gas carbon dioxide (CO_2) has increased by about 36 %, mainly as a result of anthropogenic activities such as fossil fuel combustion, land use change and cement production (Solomon et al., 2007). The increase of atmospheric CO_2 results in global warming with adverse

consequences such as rising sea levels and an increase of extreme weather conditions. Our knowledge about the sources and sinks of CO_2 has large gaps (Stephens et al., 2007). A better knowledge is required for reliable climate prediction. Previous inverse modelling studies have shown that satellite observations of the vertical column of CO_2 or of its column-averaged dry air mole-fraction, XCO_2, can deliver important information on regional CO_2 surface fluxes, which currently cannot be provided by the sparse surface networks of very accurate ground based measurements (Rayner and O'Brien, 2001; Houweling et al., 2004; Miller et al., 2007; Chevallier et al., 2007). However, this requires highly accurate satellite retrievals. As shown by Chevallier et al. (2007) and Miller et al. (2007) especially regional biases need to be avoided as even biases of a few tenths of a ppm can harm the inversion.

The grating spectrometer SCIAMACHY (SCanning Imaging Absorption spectroMeter of Atmospheric CHartographY) (Burrows et al., 1995; Bovensmann et al., 1999) on-board ENVISAT (ESA's ENVIronmental SATellite), launched in 2002, and the Fourier transform spectrometer TANSO (Thermal And Near infrared Sensor for carbon Observation) on-board GOSAT (Greenhouse gases Observing SATellite) (Yokota et al., 2004; Kuze et al., 2009), launched in 2009, are the only satellite instruments which observe backscattered near-infrared sunlight and provide measurements of CO_2 columns or XCO_2 with high sensitivity down to the Earth's surface (Buchwitz et al., 2005a,b, 2006, 2007; Houweling et al., 2005; Bösch et al., 2006; Barkley et al., 2006a,b,c, 2007; Schneising et al., 2008, 2011; Reuter et al., 2010; Yokota et al., 2004; Oshchepkov et al., 2008; Butz et al., 2009; Saito et al., 2009; Kuze et al., 2009; Yoshida et al., 2011; Morino et al., 2011) as needed for the regional CO_2 surface flux inversion application. For the period of mid 2002–March 2009, SCIAMACHY is the only satellite instrument which permits XCO_2 retrievals with high near-surface sensitivity. In addition to SCIAMACHY and GOSAT, OCO-2 (Orbiting Carbon Observatory-2) (Crisp et al., 2004; Bösch et al., 2011) and CarbonSat (Carbon Monitoring Satellite) (Bovensmann et al., 2010) are planned future satellite missions with the objective to provide additional constraints on natural CO_2 sources and sinks. Amongst CarbonSat's objectives is also the monitoring of strong localised anthropogenic CO_2 and CH_4 emissions, e.g. from coal-fired power plants and landfill sites (Bovensmann et al., 2010; Velazco et al., 2011).

In order to invert SCIAMACHY measurements to obtain XCO_2, several retrieval algorithms have been developed (Buchwitz and Burrows, 2004; Buchwitz et al., 2006, 2007; Barkley et al., 2006a; Bösch et al., 2006; Schneising et al., 2008, 2011; Reuter et al., 2010). One of them is the weighting function modified differential optical absorption spectroscopy (WFM-DOAS) retrieval algorithm (Buchwitz et al., 2000), which is based on a fast look-up-table scheme. The latest version is 2.1 (WFMDv2.1) (Schneising et al., 2011, 2012). WFMDv2.1 has been used to generate a global XCO_2 data set covering the years 2003–2009 (Schneising et al., 2011).

An important error source for satellite retrievals is unaccounted or not fully accounted scattering by aerosols and clouds. The impact of aerosols and clouds on XCO_2 or CO_2 column retrievals has been investigated in several studies mostly using simulations (Tolton and Plouffe, 2001; O'Brien and Rayner, 2002; Kuang et al., 2002; Dufour and Bréon, 2003; Buchwitz and Burrows, 2004; Christi and Stephens, 2004; Mao and Kawa, 2004; Buchwitz et al., 2005a; van Diedenhoven et al., 2005; Barkley et al., 2006a; Aben et al., 2006; Bril et al., 2007; Reuter et al., 2010), but also by analysis of measured data (Houweling et al., 2005; Schneising et al., 2008).

To minimise scattering related errors, full physics retrieval algorithms were developed which explicitly account for aerosols and clouds (Reuter et al., 2010, 2011; Butz et al., 2009, 2011). These algorithms are computationally very expensive. For SCIAMACHY, only initial results derived using these advanced algorithms are described in the peer-reviewed literature (Reuter et al., 2011). The largest multi-year global SCIAMACHY XCO_2 data set described in the peer-reviewed literature is the WFMDv2.1 XCO_2 data set.

In this study, we present an investigation of the WFMDv2.1 XCO_2 data set which we compare with CarbonTracker XCO_2. We focus on identifying and quantifying systematic retrieval errors caused by aerosols and unaccounted clouds. Schneising et al. (2008) presented an initial assessment of XCO_2 errors resulting from aerosols and clouds mostly based on simulated retrievals using WFMDv1.0 retrievals. Here we analyse WFMDv2.1 retrievals from real satellite data and discuss comparisons with global aerosol and cloud data sets based on measurements. During our investigation we have identified a scan-angle-dependent bias of the WFMDv2.1 data product. To correct for this we have developed an empirical correction method, which is described in this manuscript.

This article is organised as follows: A short overview of the WFM-DOAS algorithm is given in Sect. 2, followed by an analysis of the sensitivity of the WFM-DOAS cloud detection algorithm in Sect. 3. The global data sets used in this study are described in Sect. 4. The scan-angle-correction method and the results of a comparison of scan-angle-corrected and uncorrected SCIAMACHY XCO_2 with CarbonTracker XCO_2 are presented in Sect. 5. The main part of this manuscript, a spatial and temporal correlation analysis of SCIAMACHY minus CarbonTracker differences with global aerosol and cloud data sets, is presented in Sect. 6. Finally, a summary and conclusions are given in Sect. 7.

2 WFM-DOAS retrieval algorithm (v2.1)

The WFM-DOAS (WFMD) retrieval algorithm was developed at the University of Bremen (Buchwitz et al., 2000)

and has been continuously improved to meet the needs of the data user community (Buchwitz and Burrows, 2004; Buchwitz et al., 2005a,b; Schneising et al., 2008, 2009, 2011). A detailed description of its theoretical background can also be found in the publication of Rozanov and Rozanov (2010). Briefly, the retrieval algorithm works as follows: It uses two spectral fit windows, which cover the O_2-A absorption band from 755 nm to 775 nm and CO_2 absorption lines between 1558 nm and 1594 nm. SCIAMACHY measures these spectral regions in nadir viewing mode with a spatial resolution of typically 60 km by 30 km. The simultaneously retrieved O_2 column is used as a light path proxy for CO_2 to reduce the influence of scattering effects. WFMD is a least-squares method that scales pre-selected atmospheric vertical profiles. The logarithm of a linearised radiative transfer model is fitted to the logarithm of the measured sun-normalised radiance (see Eq. 1 of Schneising et al., 2008). The fit-parameters directly yield the desired vertical columns of CO_2 and O_2. The O_2 column is needed in order to obtain the dry air column required for the conversion of the CO_2 column into XCO_2 (Schneising et al., 2008), the final product of the WFMD algorithm. The SCIAMACHY XCO_2 algorithm not only has to be very accurate but also sufficiently fast in order to process the large amounts of data produced by SCIAMACHY. For this reason, a fast look-up-table (LUT) scheme has been developed to avoid computationally expensive radiative transfer (RT) simulations. The WFMD algorithm also includes a cloud detection algorithm, which flags cloudy ground pixels, and a surface albedo retrieval, which delivers the surface albedo of a ground pixel. Binary quality flags ("good/bad") are set a posteriori to identify successful retrievals. They are based on various criteria such as the quality of the spectral fits.

In this study, monthly means of the SCIAMACHY WFMDv2.1 XCO_2 Level 2 data product of Schneising et al. (2011) are used, which cover the time period 2003–2009. For the investigation of SCIAMACHY minus CarbonTracker differences, we only used data from the time period 2004–2008. We do not use 2003 data because of instrumental issues at the beginning of 2003 (Schneising et al., 2011). We excluded 2009 because the aerosol reference data we are using are only available until mid 2009.

2.1 WFM-DOAS and aerosols

WFMD uses a constant aerosol vertical profile for the RT simulations that does not depend on time or location. Aerosol variability is taken into account as follows: (i) by using O_2 as proxy for the light path; (ii) by the low-order polynomial included in the WFMD spectral fits, which makes the retrieval insensitive to spectrally broadband radiance modifications resulting from, for example, aerosols; and (iii) by filtering out scenes contaminated by high loads of aerosols as identified using the SCIAMACHY Absorbing Aerosol Index (AAI) (Tilstra et al., 2007) data product, which is sensitive to aerosol events such as desert dust storms, volcanic eruptions or smoke from forest fires.

Nevertheless, aerosols are still a possible source of errors. Schneising et al. (2008) performed simulations to estimate the impact of aerosols on the WFMDv1.0 XCO_2 retrievals using several aerosol scenarios. They concluded that aerosol related XCO_2 errors are typically below 1 %.

2.2 WFM-DOAS and clouds

As mentioned, clouds are an important error source for the XCO_2 data product retrieved from measurements of the upwelling solar electromagnetic radiation of the top of the atmosphere. Consequently, cloud contaminated ground scenes have to be identified and filtered out. For this purpose, WFM-DOAS includes a cloud detection algorithm, which is based on two cloud filtering criteria and filters out cloudy scenes if one of these criteria is met.

The first criterion, used to establish cloud free scenes, is based on subpixel information provided by SCIAMACHY's polarisation measurement device (PMD) 1. PMD 1 is mainly sensitive to radiation which is polarised perpendicular to the SCIAMACHY optical plane and covers the spectral ultraviolet A (UVA) region between 310 nm and 365 nm. The spatial resolution is approximately 15 km by 30 km (Bovensmann et al., 1999). In order to identify a cloud contaminated ground scene, the high cloud brightness in the UVA region is used. PMD 1 is one of seven SCIAMACHY PMD channels and has been selected because of its low sensitivity to surface albedo variations (Buchwitz et al., 2005a). If the normalised and solar zenith angle corrected PMD 1 signal exceeds a certain threshold, the ground pixel is classified as cloud contaminated (Buchwitz et al., 2005a).

The second criterion is based on a threshold for the retrieved O_2 column. The retrieved O_2 column has to be larger than 90 % of the assumed a-priori O_2 column, which is determined from surface height (pressure) and the known mixing ratio of O_2 (Schneising et al., 2008).

In the following section more details describing the cloud detection algorithm are presented along with a quantitative analysis of the sensitivity of this algorithm needed for the purpose of this study.

3 Sensitivity of the WFM-DOAS cloud detection algorithm

In order to study the influence of clouds on WFMDv2.1 XCO_2, we have to know "which clouds" remain after the application of the WFM-DOAS PMD 1 and O_2 based cloud detection algorithm. For this reason, the minimum detectable effective cloud optical depth (eCOD defined as cloud optical depth times cloud fractional coverage, i.e. "detection threshold"), which can be detected using the WFMDv2.1 cloud detection algorithm, has been determined using simulations. In

the following it is described how these PMD 1 and O_2 detection thresholds have been obtained and what their threshold values are.

The SCIAMACHY PMD signals are not yet absolutely radiometrically calibrated. To be able to determine the sensitivity of the PMD-based cloud detection algorithm using RT simulations, the PMD cloud detection threshold needs to be related to the corresponding radiance or sun-normalised radiance, also called intensity. In the following it is explained how this has been achieved.

The PMD algorithm works as follows: The uncalibrated PMD 1 signal is normalised to a fixed maximum value and divided by the cosine of the solar zenith angle (SZA). If this reflectivity-like PMD signal, SR_{PMD}, exceeds a given threshold of $SR_{PMD} = 0.7$ for at least one PMD subpixel, the SCIAMACHY pixel is flagged as cloudy. The used maximum value and the threshold have been obtained by visual inspection of SCIAMACHY PMD images (Buchwitz et al., 2005a).

In order to simulate SR_{PMD} using RT simulations, we calibrated PMD 1, i.e. we have determined the corresponding intensity in absolute physical units. For this purpose we have used the calibrated SCIAMACHY nadir intensity spectra in the corresponding wavelength region (using channel 2, cluster 9, covering the region 320 nm–365 nm). As shown in Fig. 1, the relationship between the PMD 1 signal and the mean intensity as measured by SCIAMACHY's science channel in the UVA region is linear. As can also be seen, the intensity, R_{SCI}, which corresponds to the PMD threshold $SR_{PMD} = 0.7$ is $R_{SCI} = 0.1074$. This relationship has been used in the following to assess the sensitivity of the PMD-based cloud detection algorithm to various cloud scenarios using RT simulations.

Simulated O_2 column retrievals have been used to determine the sensitivity of the O_2 column based cloud detection algorithm. This cloud detection algorithm works as follows: If the deviation between the retrieved and the a-priori O_2 column, defined as $P_{O_2} = 1 - O^{col}_{2,retrieved}/O^{col}_{2,a\text{-}priori}$ is larger than $P_{O_2} = 10\,\%$, the corresponding SCIAMACHY pixel is flagged as cloudy. For the RT simulations of the SCIAMACHY spectra, the SCIATRAN RT code (Rozanov et al., 2005) has been used.

The RT simulations are based on a standard scenario with an ice cloud. This scenario has been defined as follows: cloud top height (CTH) 10 km, cloud geometrical thickness (CGT) 500 m and fractal ice particles based on a tetrahedron with an edge length of 50 µm. Aerosols are considered by a realistic aerosol scenario (see the OPAC background scenario described in Schneising et al., 2008, 2009).

Figure 2 shows simulated R_{SCI} and O_2 column differences between retrieved and a-priori columns, P_{O_2}, for different cloud fractional coverages (CFC) as a function of cloud optical depth (COD). The simulations are valid for a surface albedo of 0.1 and a solar zenith angle (SZA) of 40°. The red lines show the PMD and O_2 cloud detection thresholds.

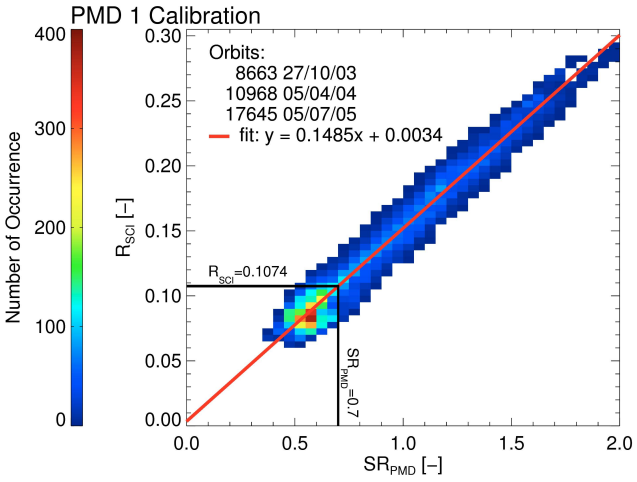

Fig. 1. Calibration of the SCIAMACHY Polarisation Measurement Device number 1 (PMD 1) signal, covering the spectral region 310–365 nm based on three orbits (see annotation). SR_{PMD} is the uncalibrated normalised PMD 1 signal divided by the cosine of the solar zenith angle (SZA). R_{SCI} is the mean reflectivity (sun-normalised radiance divided by the cosine of the SZA) as measured by SCIAMACHY in a spectral region which corresponds to the spectral region covered by PMD 1. The linear fit shows that the PMD 1 based cloud detection criterion $SR_{PMD} = 0.7$ corresponds to $R_{SCI} = 0.1074$.

The sensitivity of the cloud detection algorithm for several cloud scenarios are shown by the intersection between the simulations and the (red) PMD and O_2 threshold lines. As can be seen, minimum effective COD, i.e. the cloud detection thresholds, are 0.89 for the PMD algorithm and 0.07 for the O_2 algorithm.

This analysis has been repeated for different combinations of albedo, SZA and CTH. The results of these simulations are summarised in Table 1, which lists the sensitivities for different cloud and surface scenarios in terms of the minimum detectable eCOD. The surface scenarios correspond to the albedos of grass (UVA: 0.03; O_2-A: 0.46), water (UVA: 0.04; O_2-A: 0.02), sand (UVA: 0.01; O_2-A: 0.25) and snow (UVA: 0.97; O_2-A: 0.92), estimated from the ASTER (Advanced Spaceborne Thermal Emission and Reflection Radiometer) spectral library version 2.0 (Baldridge et al., 2009) and from the Digital Spectral Library 06 of the US Geological Survey. In addition, a constant albedo of 0.1 has been used.

The simulations yield the following results: The PMD-based algorithm filters out thick clouds and bright surfaces in the UVA region like snow. The O_2-column based algorithm is typically more sensitive, especially to high thin clouds. It needs to be pointed out that this analysis is restricted to homogeneously cloud covered ground pixels as the focus of this study is on (horizontally extended) thin cirrus clouds. Because a SCIAMACHY main channel ground pixel includes several PMD subpixel, the PMD algorithm is typically

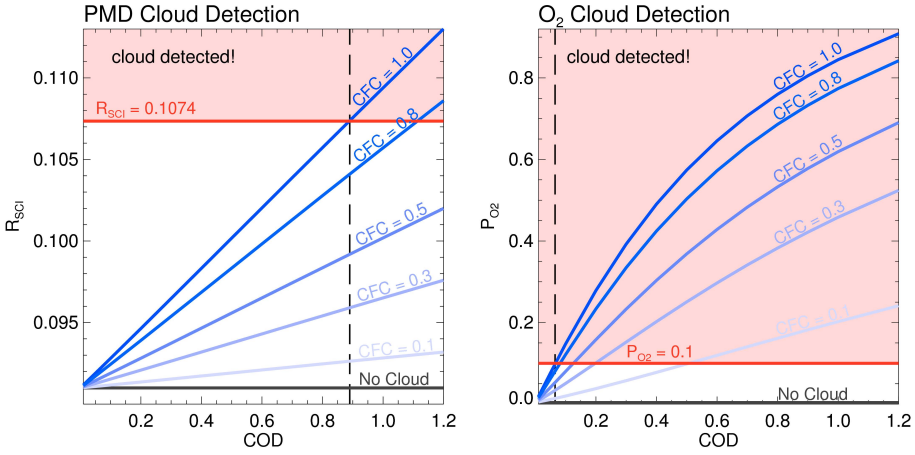

Fig. 2. PMD (given as reflectivity, left panel) and O_2 (right panel) cloud detection thresholds (red lines) compared to results obtained from radiative transfer simulations and simulated retrievals for various cloud scenarios. The left panel shows simulated reflectivity R_{SCI} for the spectral region covered by PMD 1, as a function of cloud optical depth (COD) for different cloud fractional coverages (CFC). The results are valid for a surface albedo of 0.1, the default aerosol scenario, a cloud top height (CTH) of 10 km and a cloud geometrical thickness (CGT) of 0.5 km. The red line shows the PMD cloud detection criterion of $R_{SCI} = 0.1074$ and the black dashed line shows the minimum detectable COD for CFC = 1.0. The panel on the right shows the simulated deviation of the retrieved O_2-column to the a-priori O_2-column, i.e. P_{O_2}, for the same parameters as used for the left hand side. The red line shows the O_2 cloud detection threshold $P_{O_2} = 0.1$ and the black dashed line shows the minimum detectable COD for CFC = 1.0.

more sensitive for cloud detection than indicated in Table 1. The PMD algorithm enables to detect optically thick but spatially small (i.e. subpixel) clouds (Buchwitz et al., 2005a). This aspect is not considered in this study. Table 1 shows that the sensitivity of the filter algorithms depends on the scene and on the SZA. As can be seen, thin clouds with eCOD of approximately less than 0.1 may remain undetected. This means that although a pixel is classified as cloud free by the WFMD cloud detection algorithm, it may be contaminated by optically thin clouds such as subvisual cirrus clouds.

4 Description of global reference data sets

In this section we describe global data sets which have been used for comparison with the SCIAMACHY WFMDv2.1 XCO_2 data product.

4.1 CarbonTracker XCO_2

In order to obtain estimates for CO_2 surface fluxes and global atmospheric CO_2 distributions from NOAA's (National Oceanic and Atmospheric Administration) highly accurate and precise greenhouse gas air sampling network, NOAA has developed the global CO_2 assimilation and modelling system CarbonTracker (Peters et al., 2007). For this study we use CarbonTracker version 2010 data of the years 2004–2008 obtained from http://carbontracker.noaa.gov for comparison with SCIAMACHY XCO_2. In order to consider the altitude sensitivity of the SCIAMACHY WFMD XCO_2 retrievals, we apply the WFMD XCO_2 averaging kernels to the CarbonTracker CO_2 vertical profiles. These

Table 1. Minimum detectable effective cloud optical depth (eCOD) for the PMD and O_2 based WFM-DOAS cloud detection algorithms for various scenarios as defined by surface albedo and solar zenith angle (SZA). The following settings have been used for all scenarios: aerosols: default scenario (see main text); clouds: cloud geometrical thickness CGT = 0.5 km and cloud fractional coverage CFC = 1.0. "∞" means that even clouds with large eCOD are not detected. "0.00" means that clouds are "detected" even if the scene is cloud free.

Minimum effective COD				
Scenario		CTH [km]		
Albedo/SZA		4	10	16
0.1/20°	PMD:	1.16	1.20	1.23
	O_2:	0.34	0.10	0.07
0.1/40°	PMD:	0.89	0.89	0.89
	O_2:	0.23	0.07	0.04
0.1/60°	PMD:	0.42	0.40	0.39
	O_2:	0.11	0.03	0.02
Grass/40°	PMD:	1.32	1.32	1.32
	O_2:	1.00	0.28	0.18
Sand/40°	PMD:	1.27	1.26	1.26
	O_2:	0.08	0.02	0.02
Water/40°	PMD:	1.43	1.42	1.42
	O_2:	0.53	0.15	0.10
Snow/40°	PMD:	0.00	0.00	0.00
	O_2:	∞	0.69	0.43

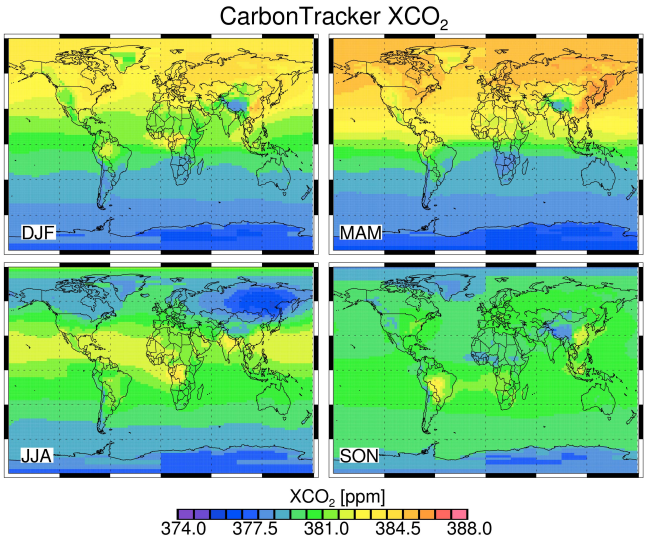

Fig. 3. Seasonal averages of NOAA's CarbonTracker XCO_2 for 2004–2008, modified to take SCIAMACHY's CO_2 column averaging kernels into account.

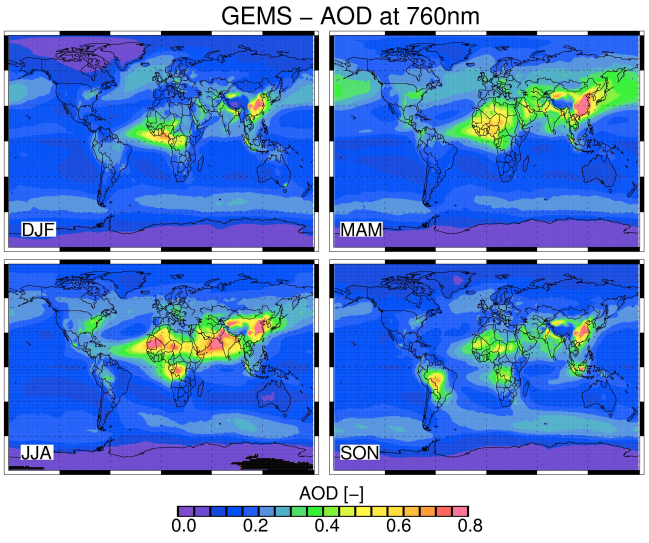

Fig. 4. Seasonal averages of aerosol optical depth (AOD) at 760 nm based on the GEMS aerosol data product of the years 2004–2008.

profiles are integrated vertically to obtain appropriate CarbonTracker XCO_2. The corresponding CarbonTracker seasonal XCO_2 averages are shown in Fig. 3. The daily CarbonTracker XCO_2 data set has been regridded on a $0.5° \times 0.5°$ longitude/latitude grid and sampled like SCIAMACHY.

4.2 Global information on aerosols

For global information on aerosols we use a data set generated within the European GEMS (Global and regional Earth-system Monitoring using Satellite and in-situ data) project (Benedetti et al., 2009; Morcrette et al., 2009). The data set has been obtained from http://data-portal.ecmwf.int/data/d/gems_reanalysis/. It covers the years 2004–2008 and provides homogeneous and consistent aerosol information in 12-h time steps time steps with full global coverage. The GEMS aerosol product is based on the assimilation of MODIS (MODerate resolution Imaging Spectroradiometer) (Barnes et al., 1998) aerosol information into a global model (Benedetti et al., 2009; Morcrette et al., 2009). For the analysis, the data set has been prepared to coincide temporally with SCIAMACHY by linear temporal interpolation. Ångström coefficients have been calculated using the original GEMS wavelengths (550 nm, 670 nm and 865 nm) and utilised to estimate aerosol optical depth (AOD) at 760 nm as needed for this study. The spatial resolution of the original data set is $1.125° \times 1.125°$. This data set has been regridded on a $0.5° \times 0.5°$ longitude/latitude grid as also done for the CarbonTracker XCO_2, as described above. Seasonal averages of the resulting AOD at 760 nm are shown in Fig. 4. For this study, the aerosol data have also been sampled like SCIAMACHY.

4.3 Global information on clouds

Global information on thin clouds derived from CALIOP (Cloud-Aerosol Lidar in Orthogonal Polarisation) on-board CALIPSO (Cloud-Aerosol Lidar and Infrared Pathfinder Satellite Observations) has been used in this study because CALIOP is sensitive to subvisual cirrus clouds (Vaughan et al., 2004; Winker et al., 2007, 2009). CALIPSO is a satellite in the A-Train constellation and was launched in April 2006. The CALIPSO data product (CAL_LID_L2_05kmCLay-Prov-V3-01) provides information on COD with a horizontal resolution of 5 km by 70 m. We have decided to use cloud statistics based on a two-year daytime CALIPSO data set (2007 and 2008), primarily due to the narrow swath of CALIPSO (70 m) compared to SCIAMACHY (960 km) and the lower spatial resolution of SCIAMACHY (30 km by 60 km).

The investigation of the sensitivity of the WFM-DOAS cloud detection algorithm presented in Sect. 3 showed that ground pixels classified cloud free may still be contaminated by thin clouds with an effective optical thickness of up to approximately eCOD = 0.1. Therefore, the CALIPSO data have been filtered to keep only scenes with COD = 0.1 or less. Using averaging and interpolation, monthly maps of COD have been generated with global coverage and a spatial resolution of $0.5° \times 0.5°$. The CALIPSO data set only provides binary information about cloud coverage. Consequently, the relative frequency of cloud occurrence has been computed for every gridbox and is used as CFC data set. Using CALIPSO derived COD and CFC, eCOD (= COD · CFC) has been computed. The corresponding seasonal averages of CALIPSO derived eCOD are shown in Fig. 5. In order to obtain daily cloud information without gaps, the monthly

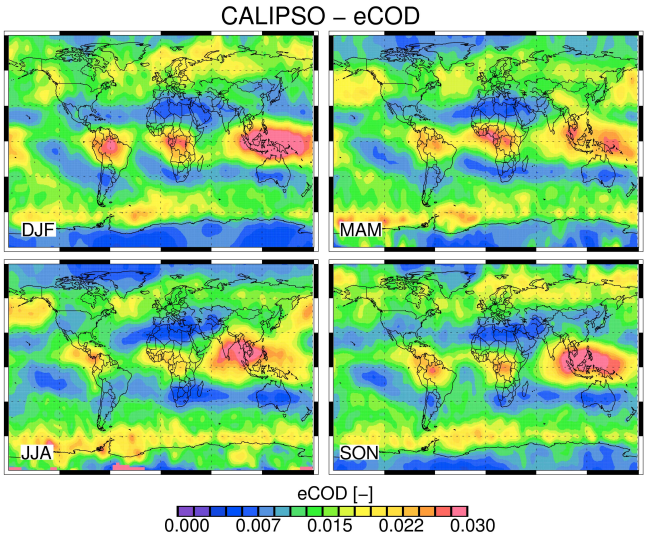

Fig. 5. Seasonal averages of effective cloud optical depth (eCOD) obtained from 2007/2008 CALIPSO/CALIOP data for clouds with COD less than 0.1.

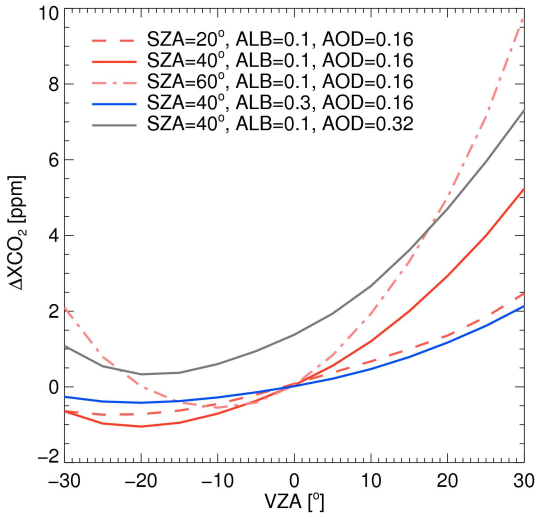

Fig. 6. Simulated systematic WFM-DOAS XCO_2 errors (ΔXCO_2) for different viewing zenith angles (VZA). The simulations are for scenarios with different solar zenith angles (SZA), surface albedos (ALB) and aerosol optical depths (AOD) at 550 nm.

data are used as daily data in the respective month. These daily CALIPSO data are sampled in the same manner as the daily data of the other data sets. The monthly means of the years 2007–2008 are used for the years 2004–2006, where no CALIPSO data are available. Note that due to the interpolation and averaging of the CALIPSO data, only statistical evidence can be given and the data set should not be used on single measurement scale.

5 Viewing geometry correction

During our investigation of the SCIAMACHY WFMDv2.1 XCO_2 data set we have found a scan-angle-dependent bias of this data product. As explained, WFM-DOAS uses a fast LUT approach to avoid time consuming RT simulations. In order to generate a manageable LUT, it is needed to limit the number of LUT elements. For this reason, the LUT was computed for exact nadir viewing conditions, i.e. only a constant viewing zenith angle (VZA), also referred to as line of sight (LOS) angle, of 0° is used. To correct for a scan-angle dependent airmass factor, a geometrical VZA correction has been implemented for the CO_2 and O_2 columns (Buchwitz and Burrows, 2004), but this does not correct the XCO_2, as this correction cancels out when the CO_2 to O_2 column ratio is computed.

As shown in Fig. 6, we have used simulated WFM-DOAS retrievals to investigate if the retrieved XCO_2 suffers from a scan-angle dependent bias. Figure 6 shows the systematic XCO_2 retrieval error as a function of VZA for different SZAs, albedos and AODs. As can be seen, the error can be as large as several ppm, especially for ground pixels with large positive VZAs (i.e. ground pixels west of the nadir position). As can also be seen, the simulations show a quadratic dependence of the systematic error on the VZA. The reason for this dependence can be unconsidered atmospheric scattering related effects.

We have analysed the SCIAMACHY retrievals based on real satellite data to find out if this error can also be observed in the WFMDv2.1 XCO_2 data product. Figure 7 shows that this is the case. Figure 7a shows global, Northern and Southern Hemispheric WFMDv2.1 XCO_2 for the years 2003–2009 as a function of the VZA. The 2D-histograms show the expected quadratic relation between the XCO_2 and the VZA. We found similar results also for smaller regions (not shown here). As can also be seen, the magnitude of the difference between the most westwards and most eastwards XCO_2 amounts to several ppm and is on the same order of magnitude as also found using simulations (see above).

In the next subsection, we present a method to correct for this bias. In the following, the original, i.e. uncorrected, SCIAMACHY XCO_2 data set is denoted as XCO_2^S, the scan-angle-corrected SCIAMACHY XCO_2 is denoted XCO_2^{S*} and the CarbonTracker XCO_2 is denoted XCO_2^C.

5.1 Correction method

Here we present an empirical scan-angle-bias correction scheme for the WFMDv2.1 data product.

SCIAMACHY scans in nadir mode across-track with viewing zenith angles (VZA) between $\pm 32°$ covering a total swath width of about 960 km. The VZA as given in the WFMDv2.1 Level 2 data product is between 0° and 32°, i.e. it is a positive number. The negative VZAs shown in Fig. 7 correspond to relative azimuth angles less than 100° (note that the azimuth angle is also given in the WFMDv2.1

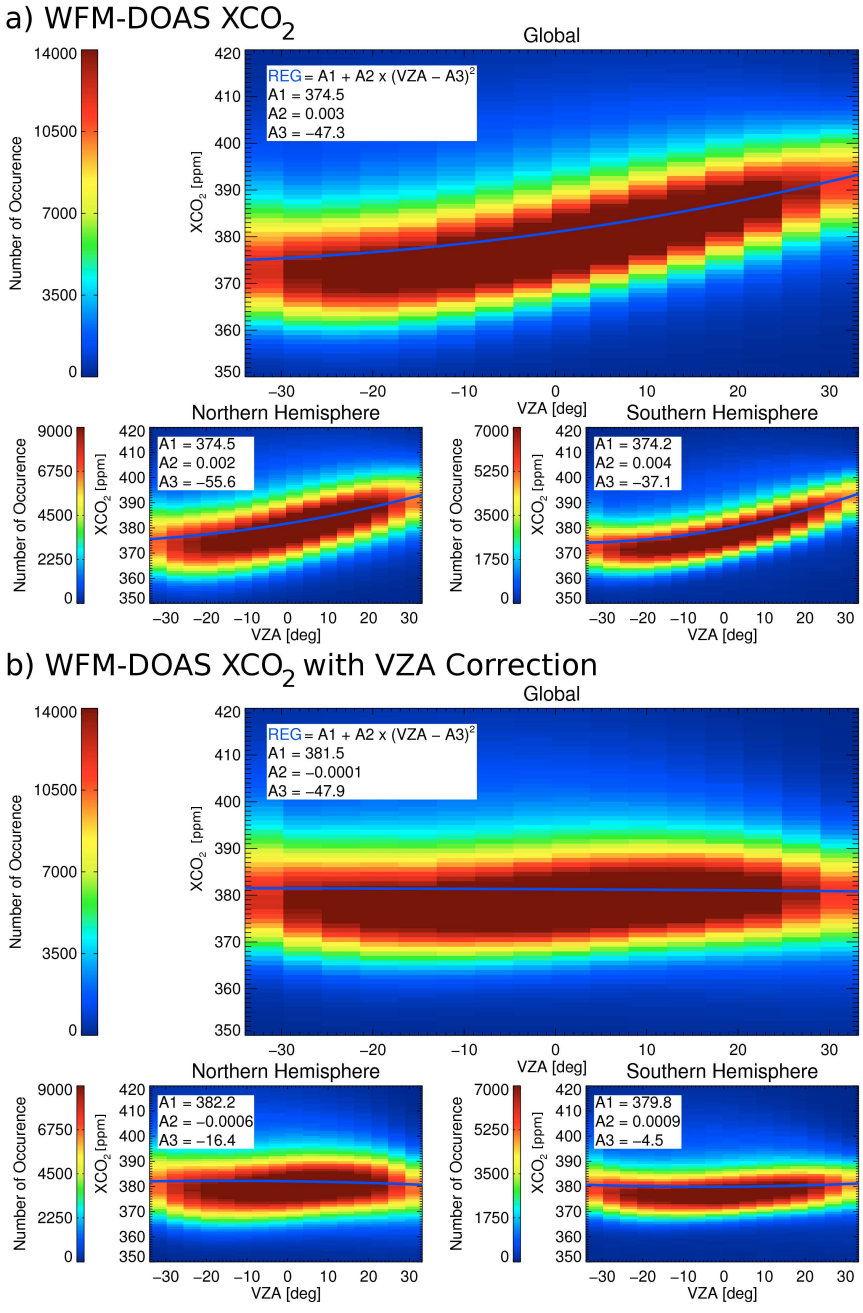

Fig. 7. WFM-DOAS XCO_2 v2.1 VZA dependency before **(a)** and after **(b)** the scan-angle-bias correction. **(a)** 2-D-histogram of WFMDv2.1 XCO_2 versus the VZA using all data between 2003 and 2009. The blue curve is a quadratic fit with fit parameters $A1$ (in ppm), $A2$ (in ppm deg^{-2}) and $A3$ (in deg). **(b)** As **(a)** but after the bias correction.

XCO_2 L2 data product and that the SZA is less than 75° for WFMD after quality filtering). Negative VZAs correspond to ground pixels east of the nadir position ("east pixel"); positive VZAs correspond to ground pixels west of the nadir position ("west pixel").

A quadratic function depending on the (signed) VZA is fitted to XCO_2^S. We have also tried other functions, e.g. a simple linear function, but a quadratic function fits best. The fit shown as blue curve in Fig. 7a is used to correct XCO_2^S in the following way:

$$XCO_2^{S*} = XCO_2^S + \Delta XCO_2^{S*-S} \quad (1)$$

$$\Delta XCO_2^{S*-S} = C1 + C2 \cdot (VZA - C3)^2. \quad (2)$$

The VZA is given in degree and XCO_2 in ppm. The numerical values of the three parameters are: $C1 = 7$ ppm,

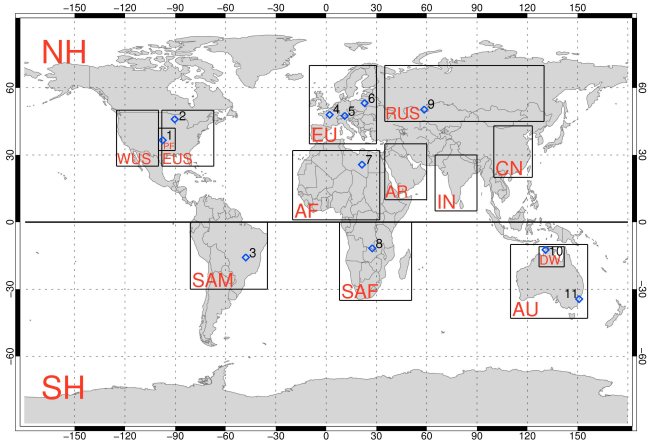

Fig. 8. Regions and locations analysed in this study (see also Tables 2 and 4).

$C2 = -0.003$ ppm deg^{-2} and $C3 = -47.3$ deg. They have been obtained from the global fit result (shown in Fig. 7a). The quality of this method is analysed in the next section.

5.2 Results

The scan-angle-bias corrected XCO_2 is shown in Fig. 7b. As can be seen, the dependency of XCO_2 on the VZA is reduced considerably, both on global (a reduction of the range of the scan-angle-dependent bias from ± 9 ppm to ± 1 ppm) and on hemispheric scales.

In order to investigate if the scan-angle-bias correction improves the SCIAMACHY WFMDv2.1 XCO_2 data set also on smaller scales, a regional comparison of corrected and uncorrected XCO_2 with CarbonTracker has been performed.

For this purpose, we have defined sixteen regions, which are shown in Fig. 8 and listed in Table 2. Monthly means of the difference between SCIAMACHY WFMDv2.1 XCO_2 and CarbonTracker XCO_2 (ΔXCO_2^{S-C}) are used to determine the influence of the scan-angle-bias correction. Figure 9 shows the impact of the scan-angle-bias correction on ΔXCO_2^{S-C} for Southern Africa. As can be seen, the time series of $\Delta XCO_2^{S^*-C}$ (red curve with corrected XCO_2) and ΔXCO_2^{S-C} (black curve with uncorrected XCO_2) differ by up to about 1 ppm and show a significant correlation (linear correlation coefficient $r = 0.89$), which indicates that the phase of the seasonality of the XCO_2 difference does not change due to the scan-angle-bias correction. The correlation coefficient between $\Delta XCO_2^{S^*-S}$ and ΔXCO_2^{S-C} is also large (-0.76). The standard deviation of the difference to CarbonTracker is smaller for the corrected (1.05 ppm) than for the uncorrected XCO_2, i.e. the agreement with CarbonTracker is better for the corrected XCO_2 for this region. The variances of the standard deviations and the square of the correlation coefficient between $\Delta XCO_2^{S^*-S}$ and ΔXCO_2^{S-C} ($r^2 = 58\,\%$) show that about 60 % of ΔXCO_2^{S-C} can be explained by the scan-angle-bias for this region.

Table 2. Latitudes and longitudes of the regions used in this study (see also Fig. 8).

Region	ID	Latitude Range	Longitude Range
Northern Hemisphere	NH	0°–90°	−180°–180°
Western USA	WUS	25°–50°	−125°–−100°
Eastern USA	EUS	25°–50°	−98°–−67°
Park Falls	PF	38°–50°	−95°–−85°
Europe	EU	35°–70°	−10°–30°
Northern Africa	AF	4°–30°	−20°–0°
Arabia	AR	10°–35°	35°–60°
Russia	RUS	45°–70°	35°–130°
India	IN	5°–30°	65°–90°
China	CN	20°–43°	100°–123°
Southern Hemisphere	SH	−90°–0°	−180°–180°
South America	SAM	−30°–0°	−81°–−35°
Southern Africa	SAF	−35°–0°	8°–51°
Australia	AU	−43°–−10°	110°–156°
Darwin	DW	−20°–−12°	127°–142°
Global	G	−90°–90°	−180°–180°

The seasonality of the scan-angle-bias correction in Southern Africa, as shown by the time series of $\Delta XCO_2^{S^*-S}$, can be explained by the following: The scan-angle-bias correction only depends on the VZA (Eq. 2). This means that a seasonality of the scan-angle-bias correction is due to a seasonality of the VZA, which originates from the quality filtering. In the winter months (large SZA), more measurements under "large" VZA conditions are filtered out than in summer (small SZA). This may be related to a higher sensitivity under "large" SZA and "large" VZA conditions (longer light path) to scattering by aerosols and clouds and/or larger noise of the spectra. Together with the VZA asymmetry of the scan-angle-bias correction (Eq. 2 and Fig. 7), this can result in the observed seasonality.

The comparison results for the other regions are shown in Table 3. The time dependence of $\Delta XCO_2^{S^*-C}$ is similar as ΔXCO_2^{S-C} for all regions. This is shown by the large correlation coefficients which are between 0.68 and 0.99. The correlation with $\Delta XCO_2^{S^*-S}$ is large for many regions, but for several Northern Hemispheric regions it is very small and/or non-significant. An example is China, shown in Fig. 10, where the large difference to CarbonTracker cannot be explained by the scan-angle related bias. The global correlation and standard deviation shows that the scan-angle-correction affects the XCO_2 data set mostly on smaller regional scales. The standard deviations of XCO_2^{S-C} are improved using the correction over all Southern Hemispheric regions and for most Northern Hemispheric regions.

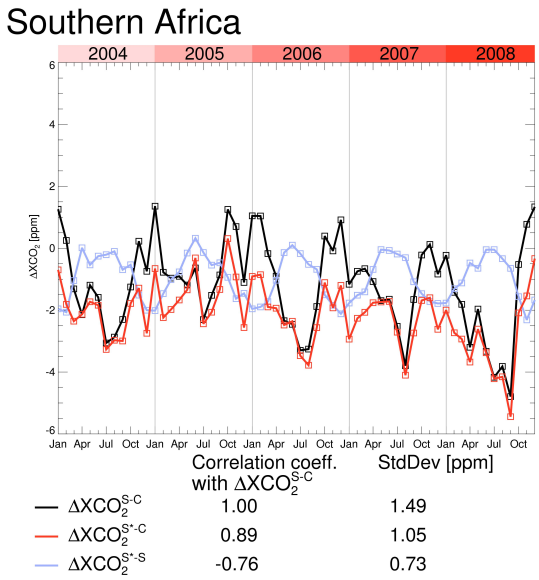

Fig. 9. Results of the comparison between CarbonTracker XCO_2 and WFMDv2.1 XCO_2 with and without scan-angle-bias correction for Southern Africa. Top: The difference between WFMDv2.1 XCO_2 and CarbonTracker XCO_2 (ΔXCO_2^{S-C}) is shown in black and the difference between the scan-angle-bias corrected WFMDv2.1 XCO_2 and CarbonTracker XCO_2 ($\Delta XCO_2^{S^*-C}$) is shown in red. The light blue curve represents the difference between scan-angle-bias corrected WFMDv2.1 XCO_2 and uncorrected XCO_2 ($\Delta XCO_2^{S^*-S}$). Bottom: correlation coefficients (r) between these differences and ΔXCO_2^{S-C} and corresponding standard deviations.

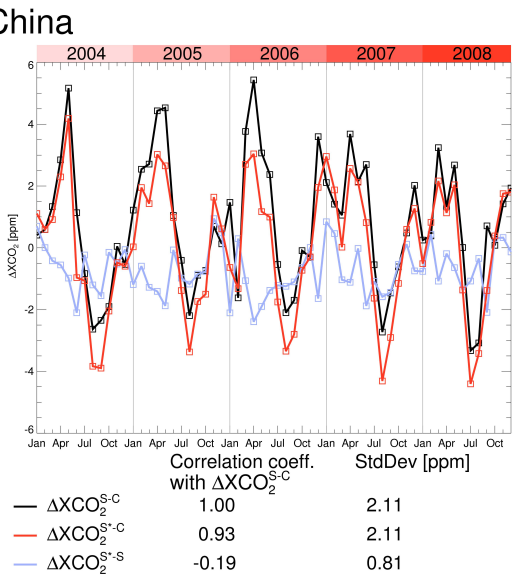

Fig. 10. As Fig. 9 but for China.

To further quantify the improvements due to the scan-angle-bias correction, we computed the standard deviation of all XCO_2 single ground pixel measurement within a radius of 350 km around several locations for each month. The location of these sites are shown in Fig. 8 and listed in Table 4. The mean values of these standard deviations may be interpreted as an upper limit of the single measurement precision (random error). The real precision is likely smaller because the standard deviations are not only due to instrument and retrieval noise but also affected by real atmospheric XCO_2 variability (note that variations due to the seasonal cycle have largely been filtered out by using standard deviations of all data in a given month) and varying systematic errors, e.g. due to the scan-angle-dependent bias. Table 4 shows absolute (in ppm) and relative (percentage) standard deviations of WFMDv2.1 XCO_2 with and without scan-angle-bias correction. As can be seen, the standard deviation is somewhat smaller for the scan-angle-bias corrected data for all locations. The intra-monthly standard deviation of XCO_2 is on average 9.04 ± 1.51 ppm for the uncorrected data and is reduced to 7.42 ± 1.29 ppm for the corrected data.

Schneising et al. (2012) validated the scan-angle-corrected SCIAMACHY XCO_2 data product against FTS (Fourier transform spectrometer) measurements of TCCON (Total Carbon Column Observing Network). They found a regional precision (defined as the mean standard deviation of the monthly differences to the TCCON FTS measurements within a radius of 500 km) of 2.1 ppm and a regional accuracy of 1.1 ppm. However, the difference to the validation results of the uncorrected XCO_2 data is not significant.

6 Analysis of SCIAMACHY-CarbonTracker XCO_2 differences due to aerosols and thin clouds

6.1 Analysis method

The three global data sets described in Sects. 4 and 5 have been used for a temporal and spatial correlation analysis: (i) the scan-angle-bias corrected SCIAMACHY-CarbonTracker difference, denoted $XCO_2^{S^*-C}$, (ii) the AOD at 760 nm as derived from the GEMS aerosol product, and (iii) CALIPSO derived eCOD.

Monthly averages are the input for the temporal correlation analysis. For the spatial analysis, averages of the four meteorological seasons (DJF, MAM, JJA and SON) of the five years 2004–2008 are used instead of monthly averages for better spatial coverage. We use these averages to reduce the scatter of the satellite data. In addition, the resolution has been reduced to $1° \times 1°$ for the spatial analysis.

In order to test whether a correlation is significant or not, a t-test is performed. For this reason, a test statistic t' based on the number of the data points n and the correlation coefficient r is computed:

$$t' = \frac{r\sqrt{n-2}}{\sqrt{1-r^2}}. \quad (3)$$

Table 3. Results of the comparison of the scan-angle-bias corrected (S*) and uncorrected (S) SCIAMACHY WFMDv2.1 XCO_2 with CarbonTracker (C). Listed are correlation coefficients (r, left) and standard deviations (right). Italic correlation coefficients are non-significant (see Sect. 6.1). The results shown are based on monthly data.

	Correlation of ΔXCO_2^{S-C} with		Standard deviation [ppm]		
Region	$\Delta XCO_2^{S^*-C}$	$\Delta XCO_2^{S^*-S}$	ΔXCO_2^{S-C}	$\Delta XCO_2^{S^*-C}$	$\Delta XCO_2^{S^*-S}$
NH	0.90	*0.04*	1.11	1.26	0.56
WUS	0.82	−0.30	1.86	1.85	1.10
EUS	0.84	−0.82	2.77	1.72	1.63
PF	0.68	−0.86	2.51	1.30	1.88
EU	0.84	*0.01*	1.43	1.72	0.94
AF	0.77	−0.64	1.17	0.90	0.75
AR	0.90	−0.45	1.59	1.42	0.68
RUS	0.80	−0.58	2.00	1.62	1.19
IN	0.99	−0.85	4.86	3.97	1.10
CN	0.93	*−0.19*	2.11	2.11	0.81
SH	0.90	−0.82	1.62	1.06	0.82
SAM	0.92	−0.67	1.96	1.54	0.80
SAF	0.89	−0.76	1.49	1.05	0.73
AU	0.71	−0.80	1.87	1.14	1.34
DW	0.95	−0.78	4.00	2.99	1.50
G	0.98	−0.23	1.14	1.11	0.22

Table 4. Monthly regional-scale scatter (in ppm and %) of the scan-angle-bias corrected (S*) and uncorrected (S) WFMDv2.1 XCO_2 data obtained from analysing all individual XCO_2 retrievals within a radius of 350 km around various locations. The numerical values are the mean standard deviations of all SCIAMACHY retrievals per month (to remove the seasonal cycle).

Monthly regional-scale scatter of the data							
ID	Location	Lat [°]	Lon [°]	XCO_2^S		$XCO_2^{S^*}$	
				[ppm]	[%]	[ppm]	[%]
1	Lamont	36.6	−97.5	9.24	2.43	7.56	1.99
2	Park Falls	46.0	−90.3	9.68	2.54	7.65	2.01
3	Brasilia	−15.8	−47.9	9.75	2.55	8.26	2.16
4	Orleans	48.0	2.1	7.69	2.01	6.28	1.64
5	Garmisch	47.5	11.1	9.53	2.51	8.09	2.14
6	Bialystok	53.2	23.0	7.62	1.99	6.09	1.59
7	Tazirbu	25.7	21.4	5.60	1.47	4.95	1.30
8	Lubumbashi	−11.7	27.5	10.72	2.82	9.09	2.39
9	Khromtau	50.3	58.5	10.77	2.83	9.23	2.43
10	Darwin	−12.4	130.9	9.42	2.47	7.21	1.89
11	Wollongong	−34.4	150.9	9.38	2.47	7.17	1.89
	Mean			9.04 ± 1.51	2.37 ± 0.40	7.42 ± 1.29	1.95 ± 0.34

To decide whether the correlation coefficient is significant or not, the resulting t' is compared with the t from a t-table, $t(f,\ p)$, which depends on the degree of freedom $f = n - 2$ and the probability value p. p is the probability that the correlation is statistically firm and is set to 95 %. If t' is larger than $t(f,\ p)$, the correlation coefficient is regarded to be significant.

6.2 Analysis results

The results of the temporal and spatial correlation analysis for China are shown in Fig. 11. The amplitude of the seasonal cycle is larger for SCIAMACHY compared to CarbonTracker. To a minor extent ($r^2 = 9.2\,\%$), the difference may be due to retrieval errors caused by thin clouds. The spatial analysis shows that in autumn, 33 % of the variability

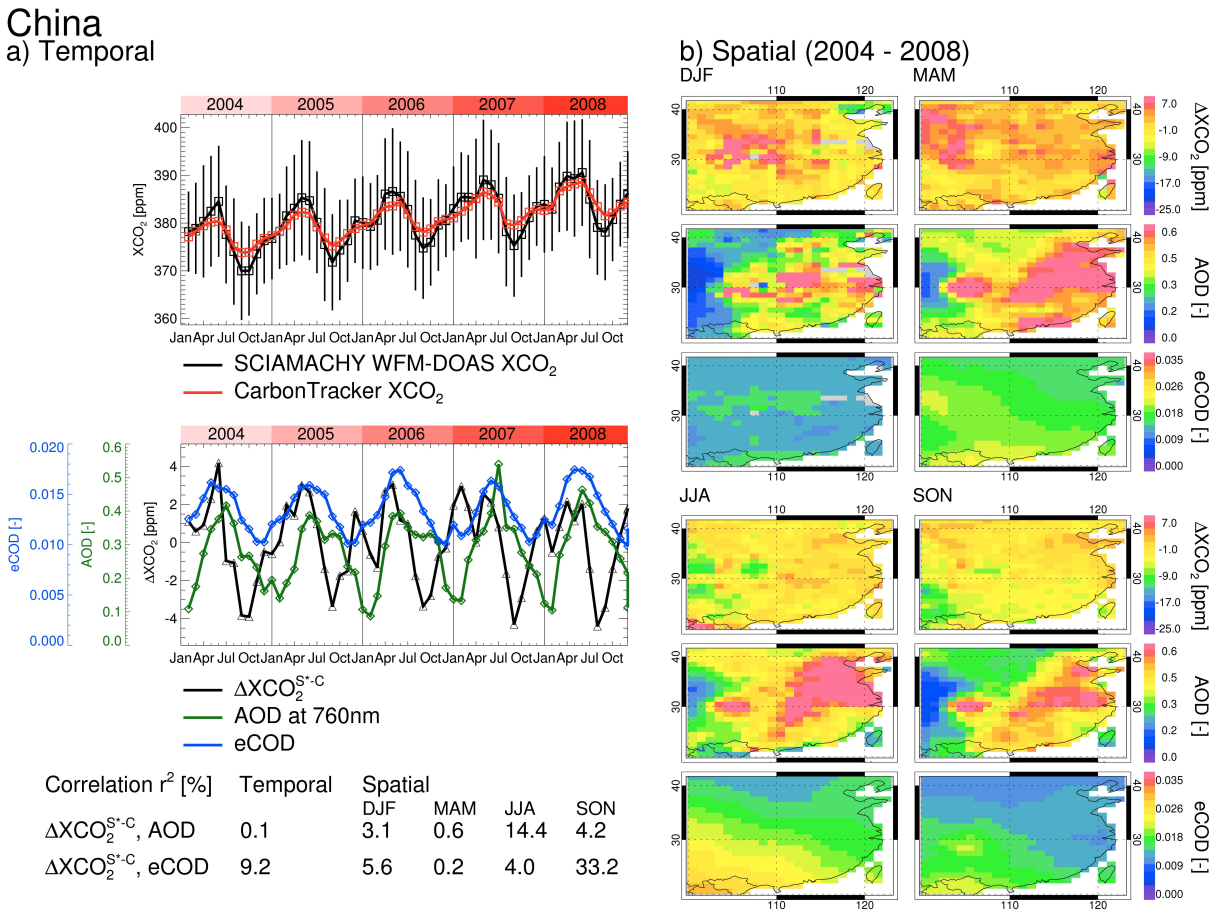

Fig. 11. Results of the temporal and spatial correlation analysis of the difference between scan-angle-corrected SCIAMACHY and CarbonTracker XCO_2, i.e. $\Delta XCO_2^{S^*-C}$, with aerosols and thin clouds for China. **(a)** Temporal analysis part: Top: The monthly means and intra-monthly standard deviations of the WFMDv2.1 XCO_2 are shown in black and CarbonTracker XCO_2 is shown in red. Middle panel: $\Delta XCO_2^{S^*-C}$ (black) compared with GEMS-derived AOD at 760 nm (green) and CALIPSO-derived eCOD (blue). Bottom left panel: The squares of the linear correlation coefficients, r^2, of the temporal and spatial correlation analysis. **(b)** Spatial analysis part: Five-year seasonal averages of $\Delta XCO_2^{S^*-C}$, AOD and eCOD.

of $\Delta XCO_2^{S^*-C}$ may be explained by eCOD, i.e. clouds related retrieval errors. The AOD over China is the highest of all investigated regions, therefore one would expect to find also the largest correlation. However, this analysis only shows low temporal and spatial correlations with aerosols. This may indicate that aerosols are not a significant problem for the WFMDv2.1 algorithm in this region. On the other hand it needs to be considered that CarbonTracker is not perfect. For example, there are indications that the underlying CASA (Carnegie-Ames Stanford Approach) biosphere model underestimates the net ecosystem exchange (NEE) between the atmosphere and the biosphere (Yang et al., 2007; Schneising et al., 2011; Keppel-Aleks et al., 2012; Messerschmidt et al., 2012). In order to investigate the impact of this underestimation on the results, we have performed the same analysis with a 40 % scaled CarbonTracker amplitude for all regions. We found that the correlations are similar for most regions and the conclusions are the same as for the unscaled CarbonTracker amplitude.

Figure 12 shows the corresponding results for Southern Africa. As can be seen, the amplitude of the difference is about 4 ppm. Neither a "U-shape", as mentioned by Schneising et al. (2008) for the seasonal cycle of the Southern Hemispheric WFMDv1.0 XCO_2, nor an evident phase shift between the seasonal cycle of $XCO_2^{S^*}$ and XCO_2^{C} can be seen in this region. However, Fig. 12 shows that 31 % of the temporal variability of $\Delta XCO_2^{S^*-C}$ may be explained by thin clouds. A larger temporal correlation ($r^2 = 55$ %) has been found for the time period 2007–2008 (the cloud statistics are based on CALIPSO measurements from these years). The temporal correlation of $\Delta XCO_2^{S^*-C}$ with aerosols is statistically not significant in this region. The spatial correlation analysis shows that there are some correlations between $\Delta XCO_2^{S^*-C}$ and eCOD and also with AOD. The largest

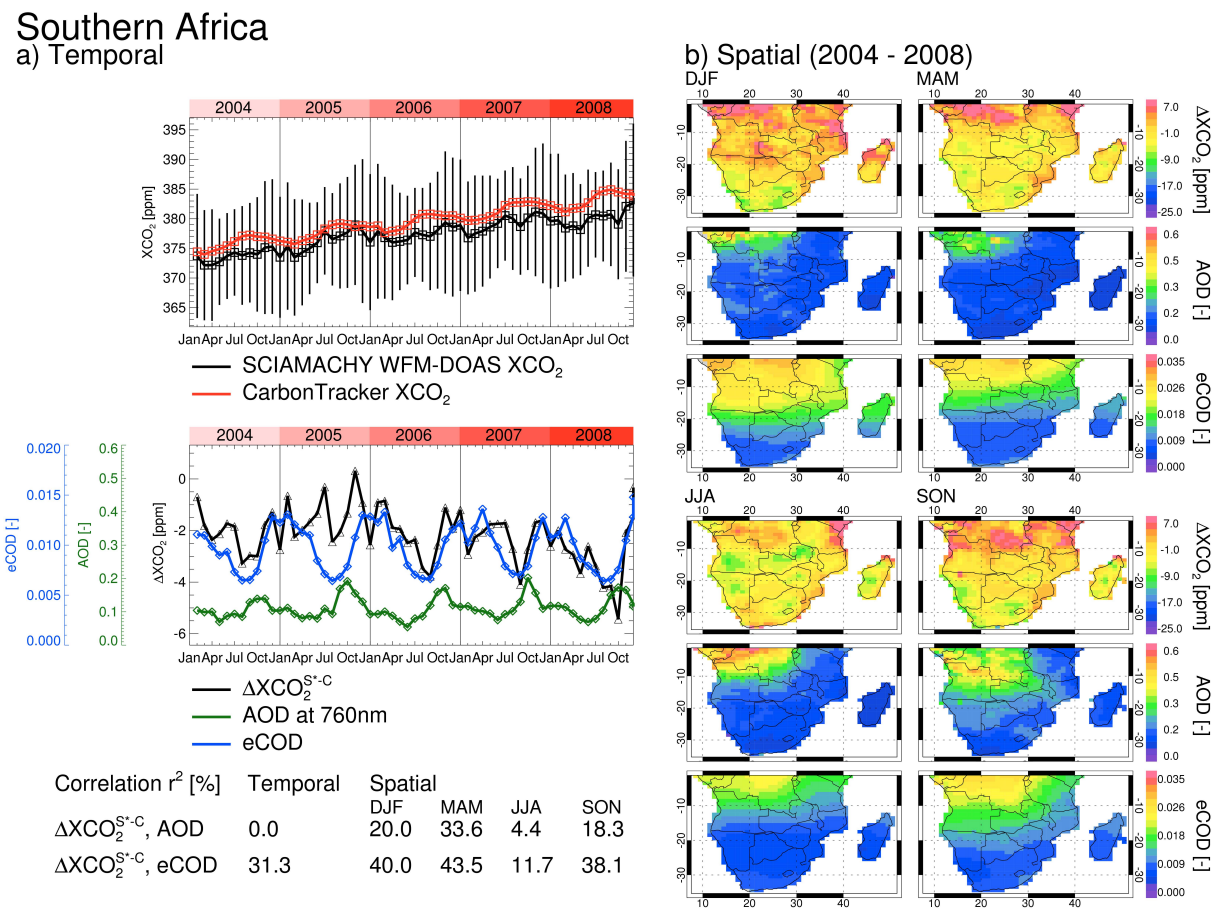

Fig. 12. As Fig. 11 but for Southern Africa.

influence of clouds and aerosols on the difference is during spring (MAM).

The corresponding results of the spatial and temporal correlation analysis for all regions investigated are summarised in Table 5. Many regions over the Northern Hemisphere show low spatial correlations ($r^2 < 25\,\%$). Due to high aerosol loads not only in China, as can be seen by the yellow to red areas in Fig. 4, e.g. over Africa, Southern Africa, Arabia and India, one would expect high spatial and temporal correlations over these regions. However, the only regions where large spatial correlations can be found are Arabia (35 % during summer), Africa (26 % during summer) and Southern Africa (34 % during spring). A large temporal correlation with aerosol can only be found for India (54 %). Large spatial correlations with thin clouds are more rarely expected than temporal correlations, e.g. due to the significant spatial smoothing of the CALIPSO data. In addition, the smoothed cloud data are based only on CALIPSO observations from the years 2007–2008. However, large spatial correlations with thin clouds are found over the Northern Hemisphere, e.g. for Africa during spring (MAM). For the Southern Hemisphere, the spatial correlations with thin clouds often exceed 25 %. The largest spatial correlation is found for Australia (48 % during DJF), indicating that a large part of the spatial variability of the XCO_2 difference in this season can be explained by thin clouds.

Temporal correlations with eCOD are typically large for several regions over the Southern Hemisphere and typically low over the Northern Hemisphere with the exception of India. Figure 5 shows that thin clouds often occur in the tropics. Therefore, one would expect the largest impact of thin clouds on the XCO_2 difference over tropical regions. This is confirmed by the correlations over India and especially over the Southern Hemisphere (most of the landmasses of the Southern Hemisphere are in the tropics). The results also corroborate the assumption of Schneising et al. (2011) that the differences between SCIAMACHY WMFDv2.1 and CarbonTracker XCO_2 over the Southern Hemisphere are likely due to unaccounted thin clouds. The low temporal and spatial correlations with aerosols for many regions show that aerosols likely only marginally contribute to the observed difference to CarbonTracker.

Table 5. Results of the spatial and temporal correlation analysis of $\Delta XCO_2^{S^*-C}$ related to aerosols (AOD) and clouds (eCOD). Italic coefficients are statistically non-significant. The coefficients, which indicate that aerosols or clouds can explain more than 25 % of the variability of $\Delta XCO_2^{S^*-C}$, are shown in bold. The results shown are based on monthly data.

Correlation coefficients r^2 [%]						
Region	Correlation of $\Delta XCO_2^{S^*-C}$ with	Temporal	Spatial			
			DJF	MAM	JJA	SON
Northern Hemisphere						
WUS	AOD:	9.0	1.7	8.4	**25.0**	5.3
	eCOD:	*3.2*	4.4	**30.3**	2.0	6.2
EUS	AOD:	7.5	7.8	1.1	0.8	4.3
	eCOD:	*1.7*	5.5	*0.2*	0.8	0.8
PF	AOD:	6.9	*1.2*	*1.1*	14.1	9.0
	eCOD:	*2.3*	*0.0*	**29.7**	**30.2**	**32.9**
EU	AOD:	*0.8*	*0.7*	1.5	*0.3*	0.6
	eCOD:	*0.4*	22.4	*0.1*	3.4	*0.3*
AF	AOD:	15.0	14.7	6.5	**26.1**	3.7
	eCOD:	*0.5*	17.3	**38.2**	2.5	0.4
AR	AOD:	18.3	*0.0*	*0.3*	**34.5**	*0.0*
	eCOD:	15.8	6.0	*0.0*	**32.9**	2.6
RUS	AOD:	20.3	*0.8*	14.6	0.4	2.4
	eCOD:	17.4	**25.0**	7.6	0.3	0.2
IN	AOD:	**54.0**	8.2	1.5	12.8	21.9
	eCOD:	**67.9**	2.0	2.5	4.9	6.9
CN	AOD:	*0.1*	3.1	0.6	14.4	4.2
	eCOD:	9.2	5.6	*0.2*	4.0	**33.2**
Southern Hemisphere						
SAM	AOD:	19.2	2.5	3.4	9.8	9.5
	eCOD:	**42.9**	19.5	15.5	1.8	14.8
SAF	AOD:	*0.0*	20.0	**33.6**	4.4	18.3
	eCOD:	**31.3**	**40.0**	**43.5**	11.7	**38.1**
AU	AOD:	*0.3*	1.4	17.3	**36.2**	19.0
	eCOD:	**28.4**	**48.4**	2.2	0.8	10.2
DW	AOD:	16.7	12.4	3.5	10.3	**34.9**
	eCOD:	**53.7**	**29.5**	**30.6**	3.4	**45.7**

7 Summary and conclusions

In this manuscript, we presented a comparison between SCIAMACHY WFM-DOAS XCO_2 and output from NOAA's assimilation and modelling system CarbonTracker to find out to what extent the observed differences between these two CO_2 data sets are influenced by systematic retrieval errors due to aerosols and unaccounted (thin) clouds. For this reason, we used the WFMDv2.1 SCIAMACHY XCO_2 data product of Schneising et al. (2011), which covers the years 2003–2009, and CarbonTracker version 2010 obtained from NOAA.

During our investigation, we found a scan-angle-dependent bias of the WFMDv2.1 XCO_2 data product. We developed an empirical correction scheme based on a parabolic function. We showed that this correction removes the scan-angle-dependent bias to a large extent and also typically results in a better agreement with CarbonTracker. We recommend to users of this data product to also apply the proposed correction scheme in order to improve the quality of the SCIAMACHY WFMDv2.1 XCO_2 data product.

We investigated to what extent the SCIAMACHY minus CarbonTracker XCO_2 differences are spatially and temporally correlated with global aerosol and cloud data sets. For

this purpose, we used a global aerosol data set generated within the European GEMS project, which is based on assimilated MODIS satellite data. For clouds, we used a data set derived from CALIPSO/CALIOP.

We found significant temporal correlations between the SCIAMACHY and CarbonTracker XCO_2 difference and CALIPSO/CALIOP effective cloud optical depth (eCOD) over the Southern Hemisphere (e.g. up to $r^2 = 54\,\%$ over Darwin, Australia). Over the Northern Hemisphere the temporal correlations with eCOD were lower or non-significant (with one exception, India, where $r^2 = 68\,\%$). Temporal correlations with aerosol optical depth (AOD) were typically lower compared to eCOD or non-significant. The spatial correlation analysis showed no clear picture over the Northern Hemisphere. Over the Southern Hemisphere, spatial correlations with clouds were often larger than 25 % (maximum: 48 % during DJF over Australia).

The correlation with thin clouds over the Southern Hemisphere corroborates the conclusion of Schneising et al. (2011) that the seasonal cycle of WFMDv2.1 XCO_2 over the Southern Hemisphere presumably suffers from unconsidered scattering due to thin clouds. This study provided more quantitative evidence that the quality of the SCIAMACHY WFMD-derived XCO_2 data product will benefit from algorithm improvements aiming at reducing cloud related retrieval errors, as described in Heymann et al. (2012), by applying an improved cloud filtering and correction method.

Acknowledgements. CarbonTracker version 2010 data were provided by NOAA ESRL, Boulder, Colorado, USA, via the website at http://carbontracker.noaa.gov. We thank the European GEMS project for the global aerosol data set. We also thank the NASA Langley Research Center Atmospheric Science Data Center for providing us with the CALIOP/CALIPSO data. We further thank the two anonymous referees and A. Galli, from SRON (Netherlands), for their helpful and valuable comments to improve this work. The research leading to the results presented in this manuscript has received funding from the European Union's Seventh Framework Programme (FP7) under Grant Agreements no. 212095 (CityZen) and 218793 (MACC), ESA (ADVANSE, CARBONGASES, GHG-CCI, SQWG), DLR (SADOS) and the University and the State of Bremen.

Edited by: H. Worden

References

Aben, I., Hasekamp, O., and Hartmann, W.: Uncertainties in the space-based measurements of CO_2 columns due to scattering in the Earth's atmosphere, J. Quant. Spectrosc. Ra., 104, 450–459, doi:10.1016/j.jqsrt.2006.09.013, 2006.

Baldridge, A. M., Hook, S., Grove, C., and Rivera, G.: The ASTER Spectral Library Version 2.0, Remote Sens. Environ., 113, 711–715, doi:10.1016/j.rse.2008.11.007, 2009.

Barkley, M. P., Frieß, U., and Monks, P. S.: Measuring atmospheric CO_2 from space using Full Spectral Initiation (FSI) WFM-DOAS, Atmos. Chem. Phys., 6, 3517–3534, doi:10.5194/acp-6-3517-2006, 2006a.

Barkley, M. P., Monks, P. S., and Engelen, R. J.: Comparison of SCIAMACHY and AIRS CO_2 measurements over North America during the summer and autumn of 2003, Geophys. Res. Lett., 33, L20805, doi:10.1029/2006GL026807, 2006b.

Barkley, M. P., Monks, P. S., Frieß, U., Mittermeier, R. L., Fast, H., Körner, S., and Heimann, M.: Comparisons between SCIAMACHY atmospheric CO_2 retrieved using (FSI) WFM-DOAS to ground based FTIR data and the TM3 chemistry transport model, Atmos. Chem. Phys., 6, 4483–4498, doi:10.5194/acp-6-4483-2006, 2006c.

Barkley, M. P., Monks, P. S., Hewitt, A. J., Machida, T., Desai, A., Vinnichenko, N., Nakazawa, T., Yu Arshinov, M., Fedoseev, N., and Watai, T.: Assessing the near surface sensitivity of SCIAMACHY atmospheric CO_2 retrieved using (FSI) WFM-DOAS, Atmos. Chem. Phys., 7, 3597–3619, doi:10.5194/acp-7-3597-2007, 2007.

Barnes, W., Pagano, T., and Salomonson, V.: Prelaunch characteristics of the Moderate Resolution Imaging Spectroradiometer (MODIS) on EOS-AM1, IEEE T. Geosci. Remote,, 36, 1088–1100, doi:10.1109/36.700993, 1998.

Benedetti, A., Morcrette, J.-J., Boucher, O., Dethof, A., Engelen, R.-J., Fisher, M., Flentje, H., Huneeus, N., Jones, L., Kaiser, J. W., Kinne, S., Mangold, A., Razinger, M., Simmons, A. J., and Suttie, M.: Aerosol analysis and forecast in the European Centre for Medium-Range Weather Forecasts Integrated Forecast System: 2. Data assimilation, J. Geophys. Res., 114, D13205, doi:10.1029/2008JD011115, 2009.

Bösch, H., Toon, G. C., Sen, B., Washenfelder, R. A., Wennberg, P. O., Buchwitz, M., de Beek, R., Burrows, J. P., Crisp, D., Christi, M., Connor, B. J., Natraj, V., and Yung, Y. L.: Space-based near-infrared CO_2 measurements: Testing the Orbiting Carbon Observatory retrieval algorithm and validation concept using SCIAMACHY observations over Park Falls, Wisconsin, J. Geophys. Res., 111, D23302, doi:10.1029/2006JD007080, 2006.

Bösch, H., Baker, D., Connor, B., Crisp, D., and Miller, C.: Global Characterization of CO_2 Column Retrievals from Shortwave-Infrared Satellite Observations of the Orbiting Carbon Observatory-2 Mission, Remote Sens. Environ., 3, 270–304, doi:10.3390/rs3020270, 2011.

Bovensmann, H., Burrows, J. P., Buchwitz, M., Frerick, J., Noël, S., Rozanov, V. V., Chance, K. V., and Goede, A.: SCIAMACHY – Mission Objectives and Measurement Modes, J. Atmos. Sci., 56, 127–150, 1999.

Bovensmann, H., Buchwitz, M., Burrows, J. P., Reuter, M., Krings, T., Gerilowski, K., Schneising, O., Heymann, J., Tretner, A., and Erzinger, J.: A remote sensing technique for global monitoring of power plant CO_2 emissions from space and related applications, Atmos. Meas. Tech., 3, 781–811, doi:10.5194/amt-3-781-2010, 2010.

Bril, A., Oshchepkov, S., Yokota, T., and Inoue, G.: Parameterization of aerosol and cirrus cloud effects on reflected sunlight spectra measured from space: application of the equivalence theorem, Appl. Optics, 46, 2460–2470, 2007.

Buchwitz, M. and Burrows, J. P.: Retrieval of CH_4, CO, and CO_2 total column amounts from SCIAMACHY near-infrared nadir spectra: Retrieval algorithm and first results, in: Remote Sens-

ing of Clouds and the Atmosphere VIII, edited by: Schäfer, K. P., Comèron, A., Carleer, M. R., and Picard, R. H., Proc. SPIE, 5235, 375–388, 2004.

Buchwitz, M., Rozanov, V. V., and Burrows, J. P.: A near-infrared optimized DOAS method for the fast global retrieval of atmospheric CH_4, CO, CO_2, H_2O, and N_2O total column amounts from SCIAMACHY Envisat-1 nadir radiances, J. Geophys. Res., 105, 15231–15245, 2000.

Buchwitz, M., de Beek, R., Burrows, J. P., Bovensmann, H., Warneke, T., Notholt, J., Meirink, J. F., Goede, A. P. H., Bergamaschi, P., Körner, S., Heimann, M., and Schulz, A.: Atmospheric methane and carbon dioxide from SCIAMACHY satellite data: initial comparison with chemistry and transport models, Atmos. Chem. Phys., 5, 941–962, doi:10.5194/acp-5-941-2005, 2005a.

Buchwitz, M., de Beek, R., Noël, S., Burrows, J. P., Bovensmann, H., Bremer, H., Bergamaschi, P., Körner, S., and Heimann, M.: Carbon monoxide, methane and carbon dioxide columns retrieved from SCIAMACHY by WFM-DOAS: year 2003 initial data set, Atmos. Chem. Phys., 5, 3313–3329, doi:10.5194/acp-5-3313-2005, 2005b.

Buchwitz, M., de Beek, R., Noël, S., Burrows, J. P., Bovensmann, H., Schneising, O., Khlystova, I., Bruns, M., Bremer, H., Bergamaschi, P., Körner, S., and Heimann, M.: Atmospheric carbon gases retrieved from SCIAMACHY by WFM-DOAS: version 0.5 CO and CH4 and impact of calibration improvements on CO_2 retrieval, Atmos. Chem. Phys., 6, 2727–2751, doi:10.5194/acp-6-2727-2006, 2006.

Buchwitz, M., Schneising, O., Burrows, J. P., Bovensmann, H., Reuter, M., and Notholt, J.: First direct observation of the atmospheric CO_2 year-to-year increase from space, Atmos. Chem. Phys., 7, 4249–4256, doi:10.5194/acp-7-4249-2007, 2007.

Burrows, J. P., Hölzle, E., Goede, A. P. H., Visser, H., and Fricke, W.: SCIAMACHY – Scanning Imaging Absorption Spectrometer for Atmospheric Chartography, Acta Astronaut., 35, 445–451, 1995.

Butz, A., Hasekamp, O. P., Frankenberg, C., and Aben, I.: Retrievals of atmospheric CO_2 from simulated space-borne measurements of backscatteres near-infrared sunlight: accounting for aerosol effects, Appl. Optics, 48, 3322–3336, 2009.

Butz, A., Guerlet, S., Hasekamp, O., Schepers, D., Galli, A., Aben, I., Frankenberg, C., Hartmann, J.-M., Tran, H., Kuze, A., Keppel-Aleks, G., Toon, G., Wunch, D., Wennberg, P., Deutscher, N., Griffith, D., Macatangay, R., Messerschmidt, J., Notholt, J., and Warneke, T.: Toward accurate CO_2 and CH_2 observations from GOSAT, Geophys. Res. Lett., 38, L14812, doi:10.1029/2011GL047888, 2011.

Chevallier, F., Bréon, F.-M., and Rayner, P. J.: Contribution of the Orbiting Carbon Observatory to the estimation of CO_2 sources and sinks: Theoretical study in a variational data assimilation framework, J. Geophys. Res., 112, D09307, doi:10.1029/2006JD007375, 2007.

Christi, M. J. and Stephens, G. L.: Retrieving profiles of atmospheric CO_2 in clear sky and in the presence of thin cloud using spectroscopy from the near and thermal infrared: a preliminary case study, J. Geophys. Res., 109, D04316, doi:10.1029/2003JD004058, 2004.

Crisp, D., Atlas, R. M., Bréon, F.-M., Brown, L. R., Burrows, J. P., Ciais, P., Connor, B. J., Doney, S. C., Fung, I. Y., Jacob, D. J., Miller, C. E., O'Brien, D., Pawson, S., Randerson, J. T., Rayner, P., Salawitch, R. S., Sander, S. P., Sen, B., Stephens, G. L., Tans, P. P., Toon, G. C., Wennberg, P. O., Wofsy, S. C., Yung, Y. L., Kuang, Z., Chudasama, B., Sprague, G., Weiss, P., Pollock, R., Kenyon, D., and Schroll, S.: The Orbiting Carbon Observatory (OCO) mission, Adv. Space Res., 34, 700–709, 2004.

Dufour, E. and Bréon, F.-M.: Spaceborn estimate of atmospheric CO_2 column by use of the differential absorption method: error analysis, Appl. Optics, 42, 3595–3609, 2003.

Heymann, J., Bovensmann, H., Buchwitz, M., Burrows, J. P., Deutscher, N. M., Notholt, J., Rettinger, M., Reuter, M., Schneising, O., Sussmann, R., and Warneke, T.: SCIAMACHY WFM-DOAS XCO_2: reduction of scattering related errors, Atmos. Meas. Tech. Discuss., 5, 4285–4320, doi:10.5194/amtd-5-4285-2012, 2012.

Houweling, S., Breon, F.-M., Aben, I., Rödenbeck, C., Gloor, M., Heimann, M., and Ciais, P.: Inverse modeling of CO_2 sources and sinks using satellite data: a synthetic inter-comparison of measurement techniques and their performance as a function of space and time, Atmos. Chem. Phys., 4, 523–538, doi:10.5194/acp-4-523-2004, 2004.

Houweling, S., Hartmann, W., Aben, I., Schrijver, H., Skidmore, J., Roelofs, G.-J., and Breon, F.-M.: Evidence of systematic errors in SCIAMACHY-observed CO_2 due to aerosols, Atmos. Chem. Phys., 5, 3003–3013, doi:10.5194/acp-5-3003-2005, 2005.

Keppel-Aleks, G., Wennberg, P. O., Washenfelder, R. A., Wunch, D., Schneider, T., Toon, G. C., Andres, R. J., Blavier, J.-F., Connor, B., Davis, K. J., Desai, A. R., Messerschmidt, J., Notholt, J., Roehl, C. M., Sherlock, V., Stephens, B. B., Vay, S. A., and Wofsy, S. C.: The imprint of surface fluxes and transport on variations in total column carbon dioxide, Biogeosciences, 9, 875–891, doi:10.5194/bg-9-875-2012, 2012.

Kuang, Z., Margolis, J., Toon, G., Crisp, D., and Yung, Y.: Spaceborne measurements of atmospheric CO_2 by high-resolution NIR spectrometry of reflected sunlight: an introductory study, Geophys. Res. Lett., 29, 1716, doi:10.1029/2001GL014298, 2002.

Kuze, A., Suto, H., Nakajima, M., and Hamazaki, T.: Thermal and near infrared sensor for carbon observation Fourier-transform spectrometer on the Greenhouse Gases Observing Satellite for greenhouse gases monitoring, Appl. Optics, 48, 6716–6733, 2009.

Mao, J. and Kawa, S. R.: Sensitivity studies for space-based measurement of atmospheric total column carbon dioxide by reflected sunlight, Appl. Optics, 43, 914–927, 2004.

Messerschmidt, J., Parazoo, N., Deutscher, N. M., Roehl, C., Warneke, T., Wennberg, P. O., and Wunch, D.: Evaluation of atmosphere-biosphere exchange estimations with TCCON measurements, Atmos. Chem. Phys. Discuss., 12, 12759–12800, doi:10.5194/acpd-12-12759-2012, 2012.

Miller, C. E., Crisp, D., DeCola, P. L., Olsen, S. C., Randerson, J. T., Michalak, A. M., Alkhaled, A., Rayner, P., Jacob, D. J., Suntharalingam, P., Jones, D. B. A., Denning, A. S., Nicholls, M. E., Doney, S. C., Pawson, S., Boesch, H., Connor, B. J., Fung, I. Y., O'Brien, D., Salawitch, R. J., Sander, S. P., Sen, B., Tans, P., Toon, G. C., Wennberg, P. O., Wofsy, S. C., Yung, Y. L., and Law, R. M.: Precision requirements for space-based X_{CO_2} data, J. Geophys. Res., 112, D10314, doi:10.1029/2006JD007659, 2007.

Morcrette, J.-J., Boucher, O., Jones, L., Salmond, D., Bechtold, P., Beljaars, A., Benedetti, A., Bonet, A., Kaiser, W., Razinger, M.,

Schulz, M., Serrar, S., Simmons, A. J., Sofiev, M., Suttie, M., Tompkins, A., and Untch, A.: Aerosol analysis and forecast in the European Centre for Medium-Range Weather Forecasts Integrated Forecast System: Forward modeling, J. Geophys. Res., 114, D06206, doi:10.1029/2008JD011235, 2009.

Morino, I., Uchino, O., Inoue, M., Yoshida, Y., Yokota, T., Wennberg, P. O., Toon, G. C., Wunch, D., Roehl, C. M., Notholt, J., Warneke, T., Messerschmidt, J., Griffith, D. W. T., Deutscher, N. M., Sherlock, V., Connor, B., Robinson, J., Sussmann, R., and Rettinger, M.: Preliminary validation of column-averaged volume mixing ratios of carbon dioxide and methane retrieved from GOSAT short-wavelength infrared spectra, Atmos. Meas. Tech., 4, 1061–1076, doi:10.5194/amt-4-1061-2011, 2011.

O'Brien, D. M. and Rayner, P. J.: Global observations of the carbon budget 2. CO_2 column from differential absorption of reflected sunlight in the 1.61 µm band of CO_2, J. Geophys. Res., 107, 4354, doi:10.1029/2001JD000617, 2002.

Oshchepkov, S., Bril, A., and Yokota, T.: PPDF-based method to account for atmospheric light scattering in observations of carbon dioxide from space, J. Geophys. Res.-Atmos., 113, D23210, doi:10.1029/2008JD010061, 2008.

Peters, W., Jacobson, A. R., Sweeney, C., Andrews, A. E., Conway, T. J., Masarie, K., Miller, J. B., Bruhwiler, L. M. P., Petron, G., Hirsch, A. I., Worthy, D. E. J., van der Werf, G. R., Randerson, J. T., Wennberg, P. O., Krol, M. C., and Tans, P. P.: An atmospheric perspective on North American carbon dioxide exchange: CarbonTracker, P. Natl. Acad. Sci., 104, 18925–18930, doi:10.1073/pnas.0708986104, 2007.

Rayner, P. J. and O'Brien, D. M.: The utility of remotely sensed CO_2 concentration data in surface inversions, Geophys. Res. Lett., 28, 175–178, 2001.

Reuter, M., Buchwitz, M., Schneising, O., Heymann, J., Bovensmann, H., and Burrows, J. P.: A method for improved SCIAMACHY CO_2 retrieval in the presence of optically thin clouds, Atmos. Meas. Tech., 3, 209–232, doi:10.5194/amt-3-209-2010, 2010.

Reuter, M., Bovensmann, H., Buchwitz, M., Burrows, J. P., Connor, B. J., Deutscher, N. M., Griffith, D. W. T., Heymann, J., Keppel-Aleks, G., Messerschmidt, J., Notholt, J., Petri, C., Robinson, J., Schneising, O., Sherlock, V., Velazco, V., Warneke, T., Wennberg, P. O., and Wunch, D.: Retrieval of atmospheric CO_2 with enhanced accuracy and precision from SCIAMACHY: Validation with FTS measurements and comparison with model results, J. Geophys. Res., 116, D04301, doi:10.1029/2010JD015047, 2011.

Rozanov, A., Rozanov, V., Buchwitz, M., Kokhanovsky, A., and Burrows, J.: SCIATRAN 2.0 – A new radiative transfer model for geophysical applications in the 175–2400 nm spectral region, in: Atmospheric remote sensing: Earth's surface, troposphere, stratosphere and mesosphere – I, edited by: Burrows, J. and Eichmann, K., vol. 36 of Adv. Space Res., doi:10.1016/j.asr.2005.03.012, 35th COSPAR Scientific Assembly, 18–25 Juky 2004, Paris, France, 1015–1019, 2005.

Rozanov, V. V. and Rozanov, A. V.: Differential optical absorption spectroscopy (DOAS) and air mass factor concept for a multiply scattering vertically inhomogeneous medium: theoretical consideration, Atmos. Meas. Tech., 3, 751–780, doi:10.5194/amt-3-751-2010, 2010.

Saito, N., Imasu, R., Ota, Y., and Niwa, Y.: CO_2 retrieval algorithm for the thermal infrared spectra of the Greenhouse Gases Observing Satellite: Potential of retrieving CO_2 vertical profile from high-resolution FTS sensor, J. Geophys. Res., 114, D17305, doi:10.1029/2008JD011500, 2009.

Schneising, O., Buchwitz, M., Burrows, J. P., Bovensmann, H., Reuter, M., Notholt, J., Macatangay, R., and Warneke, T.: Three years of greenhouse gas column-averaged dry air mole fractions retrieved from satellite – Part 1: Carbon dioxide, Atmos. Chem. Phys., 8, 3827–3853, doi:10.5194/acp-8-3827-2008, 2008.

Schneising, O., Buchwitz, M., Burrows, J. P., Bovensmann, H., Bergamaschi, P., and Peters, W.: Three years of greenhouse gas column-averaged dry air mole fractions retrieved from satellite – Part 2: Methane, Atmos. Chem. Phys., 9, 443–465, doi:10.5194/acp-9-443-2009, 2009.

Schneising, O., Buchwitz, M., Reuter, M., Heymann, J., Bovensmann, H., and Burrows, J. P.: Long-term analysis of carbon dioxide and methane column-averaged mole fractions retrieved from SCIAMACHY, Atmos. Chem. Phys., 11, 2863–2880, doi:10.5194/acp-11-2863-2011, 2011.

Schneising, O., Bergamaschi, P., Bovensmann, H., Buchwitz, M., Burrows, J. P., Deutscher, N. M., Griffith, D. W. T., Heymann, J., Macatangay, R., Messerschmidt, J., Notholt, J., Rettinger, M., Reuter, M., Sussmann, R., Velazco, V. A., Warneke, T., Wennberg, P. O., and Wunch, D.: Atmospheric greenhouse gases retrieved from SCIAMACHY: comparison to ground-based FTS measurements and model results, Atmos. Chem. Phys., 12, 1527–1540, doi:10.5194/acp-12-1527-2012, 2012.

Solomon, S., Qin, D., Manning, M., Chen, Z., Marquis, M., Averyt, K. B., Tignor, M., and Miller, H. L. (Eds.): Climate change 2007: The physical science basis, Contribution of working group I to the Fourth Assessment Report of the Intergovernmental Panel on Climate Change – IPCC, Cambridge University Press, 2007.

Stephens, B. B., Gurney, K. R., Tans, P. P., Sweeney, C., Peters, W., Bruhwiler, L., Ciais, P., Ramonet, M., Bousquet, P., Nakazawa, T., Aoki, S., Machida, T., Inoue, G., Vinnichenko, N., Lloyd, J., Jordan, A., Heimann, M., Shibistova, O., Langenfelds, R. L., Steele, L. P., Francey, R. J., and Denning, A. S.: Weak northern and strong tropical land carbon uptake from vertical profiles of atmospheric CO_2, Science, 316, 1732–1735, doi:10.1126/science.1137004, 2007.

Tilstra, L. G., de Graaf, M., Aben, I., and Stammes, P.: Analysis of 5 years of SCIAMACHY absorbing aerosol index data, Proceedings ENVISAT Symposium, Montreux, Switzerland, ESA Special Publication SP-636, 2007.

Tolton, B. T. and Plouffe, D.: Sensitivity of radiometric measurements of the atmospheric CO_2 column from space, Appl. Optics, 40, 1305–1313, 2001.

van Diedenhoven, B., Hasekamp, O. P., and Aben, I.: Surface pressure retrieval from SCIAMACHY measurements in the O_2 A Band: validation of the measurements and sensitivity on aerosols, Atmos. Chem. Phys., 5, 2109–2120, doi:10.5194/acp-5-2109-2005, 2005.

Vaughan, M., Young, S., Winker, D., Powell, K., Omar, A., Liu, Z., Yongxiang, H., and Hostetler, C.: Fully automated analysis of space-based lidar data: an overview of the CALIPSO retrieval algorithms and data products, Laser Radar Tech. Atmos. Sens., 5575, 16–30, doi:10.1117/12.572024, 2004.

Velazco, V. A., Buchwitz, M., Bovensmann, H., Reuter, M., Schneising, O., Heymann, J., Krings, T., Gerilowski, K., and Burrows, J. P.: Towards space based verification of CO_2 emissions from strong localized sources: fossil fuel power plant emissions as seen by a CarbonSat constellation, Atmos. Meas. Tech., 4, 2809–2822, doi:10.5194/amt-4-2809-2011, 2011.

Winker, D. M., Hunt, W. H., and McGill, M. J.: Initial performance assessment of CALIOP, Geophys. Res. Lett., 34, L19803, doi:10.1029/2007GL030135, 2007.

Winker, D., Vaughan, M., Omar, A., Hu, Y., Powell, K. A., Liu, Z., Hunt, W., and Young, S.: Overview of the CALIPSO Mission and CALIOP Data Processing Algorithms, J. Atmos. Ocean. Tech., 26, 2310–2323, 2009.

Yang, Z., Washenfelder, R. A., Keppel-Aleks, G., Krakauer, N. Y., Randerson, J. T., Tans, P. P., Sweeney, C., and Wennberg, P. O.: New constraints on Northern Hemisphere growing season net flux, Geophys. Res. Lett., 34, L12807, doi:10.1029/2007GL029742, 2007.

Yokota, T., Oguma, H., Morino, I., and Inoue, G.: A nadir looking SWIR sensor to monitor CO_2 column density for Japanese GOSAT project, Proceedings of the twenty-fourth international symposium on space technology and science, Miyazaki: Japan Society for Aeronautical and Space Sciences and ISTS, 887–889, 2004.

Yoshida, Y., Ota, Y., Eguchi, N., Kikuchi, N., Nobuta, K., Tran, H., Morino, I., and Yokota, T.: Retrieval algorithm for CO_2 and CH_4 column abundances from short-wavelength infrared spectral observations by the Greenhouse gases observing satellite, Atmos. Meas. Tech., 4, 717–734, doi:10.5194/amt-4-717-2011, 2011.